SUPPLEMENTARY DATA

TABLES

Table S1. Apparent *Kd* values of recombinases [a]

Construct	Nucleotide	Apparent K_d (μM)
RAD51 WT	**apo**	< 0.17
	ATP	< 0.55
	AMP-PNP	< 0.18
	ADP	< 1.0
	apo (3')	< 0.37
	ATP (3')	< 0.33
	Ca-ATP	< 0.33
RAD51 KR	**apo**	< 2.6
	ATP	< 0.44
RAD51 KA	**apo**	< 0.28
	ATP	< 1.5
RecA	**apo**	< 0.31
	ATP	< 1.1
	AMP-PNP	< 0.12
yRad51	**apo**	weak binding (> 2 μM)
	ATP	< 0.21
	AMP-PNP [b]	cooperative binding (K_d = 1.8 – 2.5 μM, n = 2.0 – 4.1)

[a] upper bound from 95 % confidence is shown for global fits to all fluorescence amplitude data, based on Eq. S2.

[b] Results of fits based on the Hill equation (Eq. S3). *n* indicates Hill coefficient.

EQUATIONS

Eq. S1: Multiexponential equation

$$F(t) = F_{\mathrm{end}} + \sum_{\mathrm{i}=1}^{\mathrm{n}} A_{\mathrm{i}} e^{-k_{\mathrm{i}} t}$$

where $F(t)$ is the fluorescence signal at time point t, F_{end} is the fluorescence end signal, and A_{i} and k_{i} are the amplitude and observed rate constant values of individual exponential phases, respectively (n = 1-3).

Eq. S2: Quadratic binding equation

$$y([\mathrm{R}]) = y_0 + (y_{\mathrm{end}} - y_0)\frac{[\mathrm{R}] + [\mathrm{D}] + K_{\mathrm{d}} - \sqrt{([\mathrm{R}] + [\mathrm{D}] + K_{\mathrm{d}})^2 - 4[\mathrm{R}][\mathrm{D}]}}{2[\mathrm{D}]}$$

where y_0 and y_{end} are the values of the recombinase concentration-dependent variable at zero and infinite recombinase concentration, respectively (floating parameters); [R] is recombinase concentration expressed in monomers (independent variable); [D] is the total concentration of recombinase binding sites on ssDNA (floating parameter; expressed in the same concentration unit as [R]); and K_d is the dissociation constant (floating parameter). The apparent ssDNA binding stoichiometry of the recombinase (Supplementary Table S1; expressed in nt/recombinase monomer) was calculated as $[D]_{nt}/[D]$ where $[D]_{nt}$ is the total applied 5'-Cy3-dT_{79} or 3'-Cy3-dT_{79} concentration expressed in nt.

Eq. S3: Hill equation

$$y([\mathrm{R}]) = y_0 + (y_{\mathrm{end}} - y_0)\frac{[\mathrm{R}]^n}{[\mathrm{R}]^n + K_{\mathrm{d}}^n}$$

where y_0 and y_{end} are the values of the recombinase concentration-dependent variable at zero and infinite recombinase concentration, respectively (floating parameters); [R] is recombinase concentration expressed in monomers (independent variable), K_d is the dissociation constant (floating parameter), and n is the Hill coefficient (floating parameter). Fit to the yRad51.AMP-PNP curve shown in Figure 5D yielded K_d = 2.1 ± 0.1 μM and n = 3.1 ± 0.5.

METHODS

ATP hydrolysis was measured as previously described in (1) by a phosphate detection system (Innova Biosciences), with 2 μM RAD51 and 100 μM ATP in the presence or absence of ssDNA. TNP-ATP binding was recorded as reported in (1) by monitoring the fluorescence emission intensity of TNP-ATP (0.5 μM) upon preincubation with RAD51 proteins (5 min, 37 ºC). All reactions were performed in SF buffer.

REFERENCES

1. Zadorozhny, K., Sannino, V., Beláň, O., Mlčoušková, J., Špírek, M., Costanzo, V., Krejčí, L. (2017) Fanconi-Anemia-Associated Mutations Destabilize RAD51 Filaments and Impair Replication Fork Protection. *Cell Rep*, **21(2)**, 333-340

SUPPLEMENTARY FIGURES

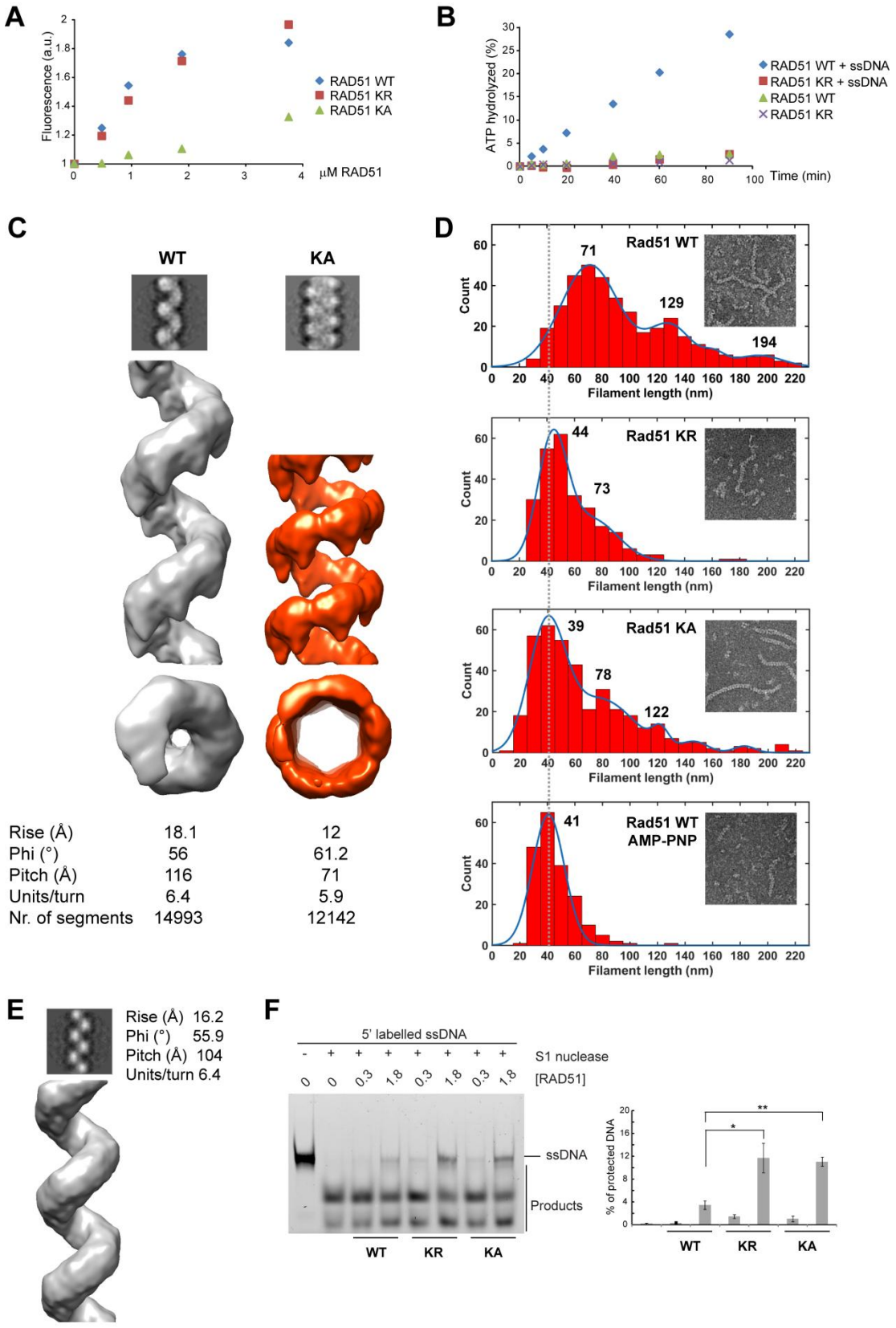

Supplementary Figure S1. Biochemical analysis of human RAD51 filaments. (**A**) ATP binding detected as a change of the fluorescence emission intensity of TNP-ATP (0.5 μM) upon binding to

RAD51 (**B**) ATP hydrolysis measured by the colorimetric phosphate detection assay with or without ssDNA (**C**) Cryo-EM reconstructions. Representative class-averages, three-dimensional reconstructions and helical parameters of cryo-electron microscopy data of RAD51 WT and KA NFs formed on short single-stranded DNA (150-mer) in the presence of ATP. (**D**) Length analysis of RAD51 filaments. Distribution of filament lengths (nm) formed by RAD51 WT, KR or KA proteins in the presence of ATP and WT in AMP-PNP upon binding single-stranded 150-mer. Insets show examples of experimental data. Bar size represents 50 Å. (**E**) 3D reconstruction obtained for RAD51 WT in 25 mM HEPES, pH 7.5, 25 mM KCl, 4 mM MgCl2, 4 mM AMP-PNP, incubated at 37 °C for 60 minutes. (**F**) S1 nuclease protection assay on protein-DNA complexes formed by RAD51 and walker box mutants with ssDNA in the presence of ATP. Errors bars indicate s.d. (n = 3).

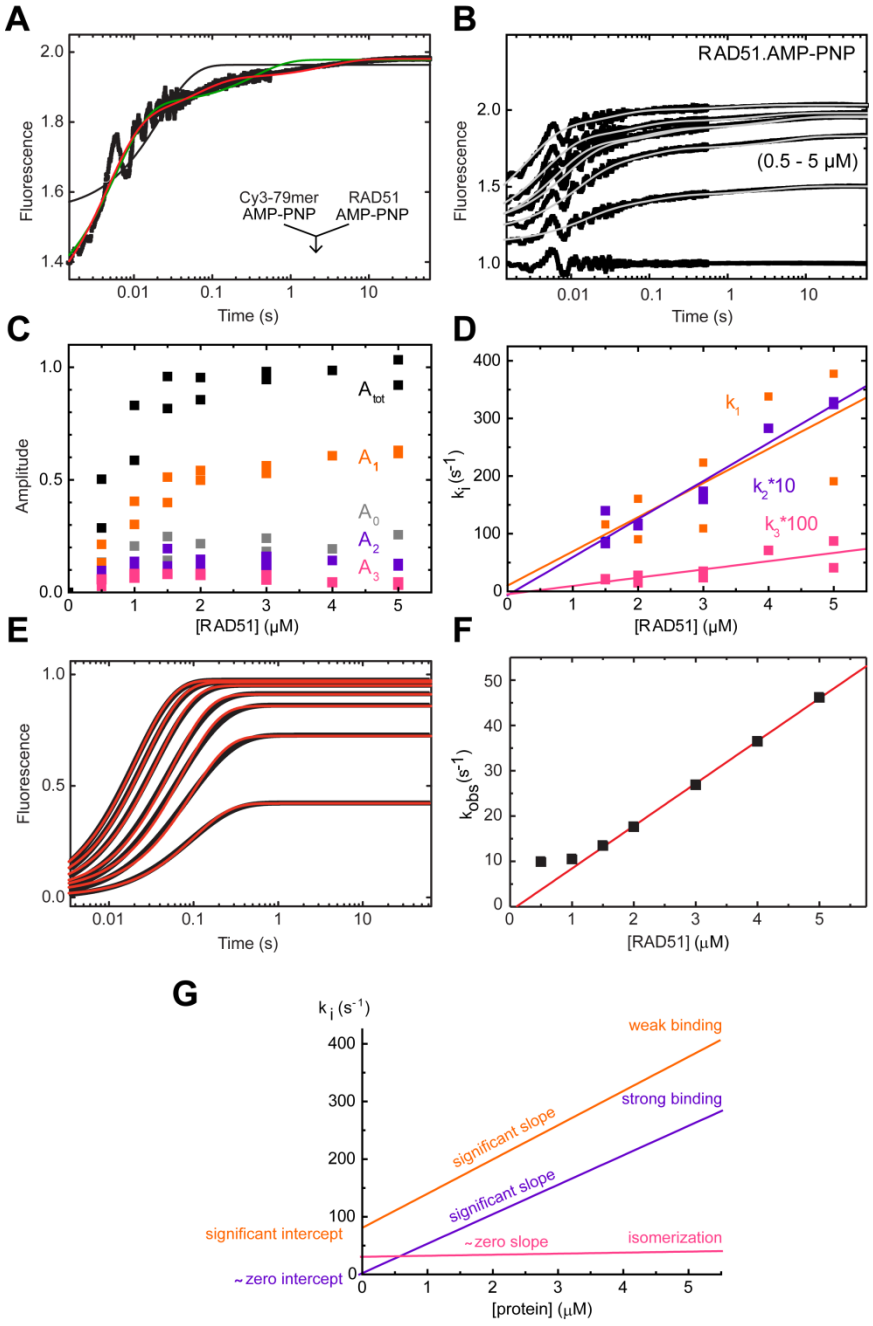

Supplementary Figure S2. Rapid kinetics of RAD51 filament formation. (**A**) Multiexponential fits to RAD51-ssDNA association transients. Mono- (black), bi- (green) and triexponential (red) fits to the trace recorded on rapidly mixing 3 μM RAD51, 1 mM AMP-PNP and 40 nM 5'-Cy3-dT_{79} (black dots) (Eq. S1). Mono- and biexponential fits showed systematic deviation from the data. (**B**) Stopped-flow Cy3 fluorescence traces recorded upon rapidly mixing 40 nM 5'-Cy3-dT_{79} (3.16 μM nt) with increasing concentrations of RAD51 (bottom to top: 0, 0.5, 1, 1.5, 2, 3, and 5 μM; post-mixing concentrations stated and expressed as monomers) after pre-incubation with 1 mM AMP-PNP. Fluorescence levels are shown relative to that of RAD51-free 5'-Cy3-dT_{79}. Tri-exponential best-fits are shown in grey. (**C**) RAD51 concentration dependence of amplitudes (A_i) of exponential phases in panel **B**, expressed relative to the fluorescence level of RAD51-free 5'-Cy3-dT_{79}. Also shown are amplitudes of the rapid fluorescence increase (A_0) occurring within the dead time of the measurement (1 ms). Quadratic fits

(Eq. S2) to the total amplitudes (A_{tot}) were used to determine the affinity of the RAD51-ssDNA interaction (Figure 3B, Supplementary Table S1). (**D**) RAD51 concentration dependence of observed rate constants (k_i) of individual exponential phases in panel **B**. For visibility, values for k_2 and k_3 were multiplied as indicated. Linear fits in the >1.5 µM RAD51 concentration regime (global fits to all rate constant data of a given kinetic phase) were used to determine the slopes and intercepts shown in Figure 3C. (**E**) Kinetic simulation of a single-step association reaction. Simulated time courses (black) and single exponential best-fits (red; Eq. S1) of a single-step association reaction between RAD51 (bottom to top: 0.5, 1, 1.5, 2, 3, 4, and 5 µM) and ssDNA (1 µM RAD51 binding sites) with a k_{on} of 10 $\mu M^{-1}s^{-1}$ and a k_{off} of 0 s^{-1}. (**F**) RAD51 concentration dependence of best-fit k_{obs} values (squares) from panel **E**. Linear fit to the data (red line) in the RAD51 concentration regime ≥ 1.5 µM yielded a slope of 9.4 ± 0.1 $\mu M^{-1}s^{-1}$. This analysis supports that linear fits can be reliably used in the applied concentration regime to estimate association kinetic parameters. (**G**) Schematic representation of observed rate constants (k_i) of exponential phases related to concentration of protein with plots representing different binding modes.

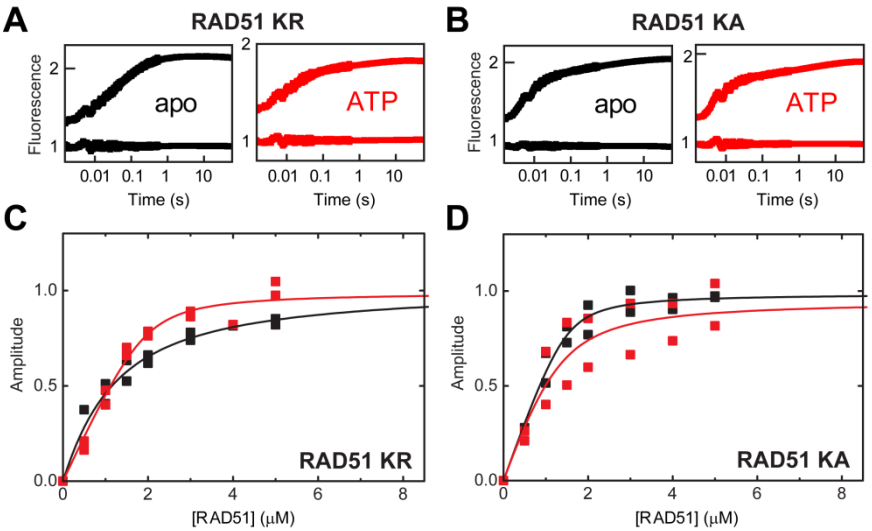

Supplementary Figure S3. Rapid kinetics of RAD51 Walker mutants filament formation. **(A, B)** Stopped-flow Cy3 fluorescence traces recorded upon rapidly mixing 40 nM 5'-Cy3-dT_{79} (3.16 µM nt) with RAD51 KR (**A**) or KA (**B**) (bottom to top: 0 and 5 µM) in the absence (apo) or presence of 1 mM ATP. Fluorescence levels are shown relative to that of RAD51-free 5'-Cy3-dT_{79}. (**C, D**) Concentration dependence of recorded total fluorescence changes for RAD51 KR (**C**) or KA (**D**) are shown relative to the extrapolated maxima of individual datasets. Kd values (determined from quadratic fits (solid lines) based on **Eq. S2**) are listed in Supplementary Table S1.

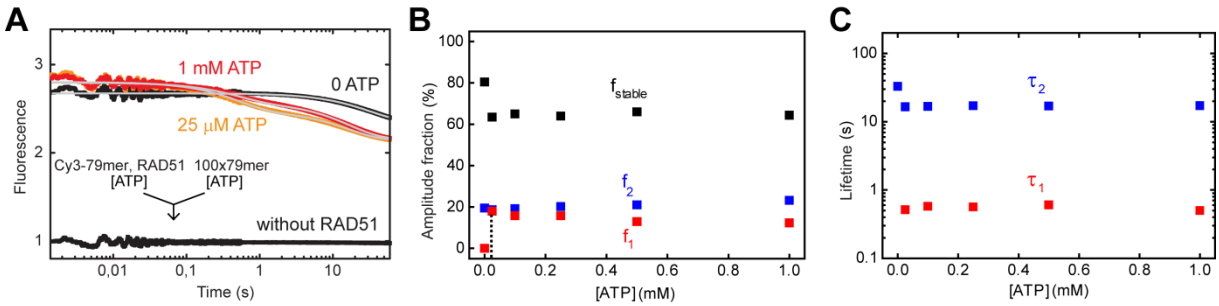

Supplementary Figure S4. Rapid kinetic traces of human RAD51 dissociation from ssDNA. (**A**) RAD51 (5 μM) was preincubated with different concentrations of ATP (as indicated) and 40 nM 5'-Cy3-dT_{79} (3.16 μM nt), followed by rapid mixing in the stopped-flow with 4 μM (316 μM nt) unlabeled dT_{79} (post-mixing concentrations stated). Transient Cy3 fluorescence levels are shown relative to that of RAD51-free 5'-Cy3-dT_{79} ("without RAD51" trace). Mono- (0 ATP trace) or biexponential (ATP traces) best-fits (**Eq. S1**) are shown as gray lines. (**B**) ATP concentration dependence of amplitude fractions (f_i) of exponential phases in experiments as in panel **A**. f_{stable} indicates stable fraction showing no sign of dissociation within the 60-s observation period (cf. panel **A**). Dashed line denotes concentration of ATP where maximal amplitude f_1 was already reached. (**C**) ATP concentration dependence of observed lifetimes (τ_1, τ_2) of exponential phases.

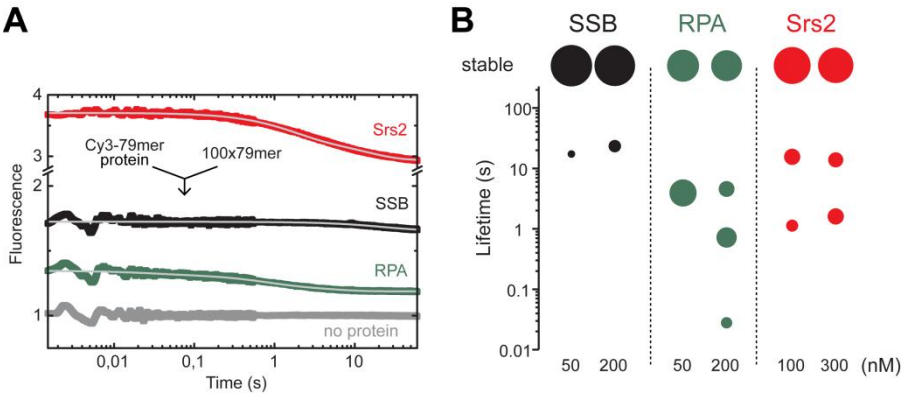

Supplementary Figure S5. (A) Rapid kinetic traces of *E. coli* SSB (200 nM), human RPA (200 nM) and yeast Srs2 (300 nM) protein dissociation from ssDNA. Proteins were preincubated with 40 nM 5'-Cy3-dT_{79} (3.16 μM nt), followed by rapid mixing in the stopped-flow with 4 μM (316 μM nt) unlabeled dT_{79} (post-mixing concentrations stated). Transient Cy3 fluorescence levels are shown relative to that of protein-free 5'-Cy3-dT_{79} ("no protein" trace). Exponential best-fits (**Eq. S1**) are shown as gray lines. **(B)** Distribution of lifetime components ($\tau_i = 1/k_i$ values) of dissociation transients in experiments performed as in panel **A**. Areas of symbols are proportional to A_i values.

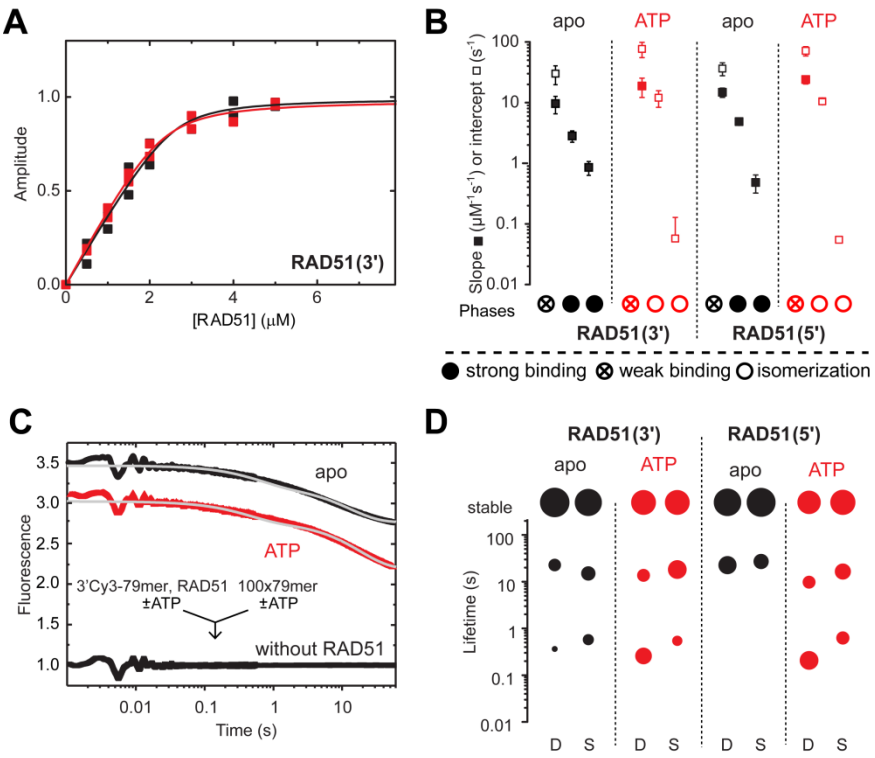

Supplementary Figure S6. RAD51 NF formation and dissociation using 3'-labeled ssDNA. (**A**) Dependence of fluorescence amplitudes of RAD51-ssDNA association transients. Total fluorescence changes are shown relative to the extrapolated maximal amplitude of individual datasets. Kd values (determined from quadratic fits (solid lines) based on Eq. S2) are listed in Supplementary Table S1. (**B**) Association kinetic parameters determined as in Supplementary Figure 2D (cf. Figure 3C for 5'-Cy3-dT_{79} data) together with symbol representation of results. Consecutive phases at given condition are indicated by circles. Strong binding: significant slope, zero intercept (solid circle). Weak binding: both the slope and intercept are significantly different from 0 (crossed circle). Isomerization: Slope is not significantly different from 0 (empty circle). Error bars show standard errors of global fits to all rate constant data of a given kinetic phase. **(C)** Rapid kinetic traces of RAD51 dissociation from 3'-labeled ssDNA. RAD51 (5 μM) was preincubated with 40 nM 5'-Cy3-dT_{79} (3.16 μM nt) in the absence (apo) and presence of ATP, followed by rapid mixing in the stopped-flow with 4 μM (316 μM nt) unlabeled dT_{79} (post-mixing concentrations stated). Transient Cy3 fluorescence levels are shown relative to that of RAD51-free 3'-Cy3-dT_{79} ("without RAD51" trace). (**D**) Lifetime components of RAD51 dissociation transients (cf. Figure 4B). Distribution of lifetimes ($\tau_i = 1/k_i$ values, cf. Eq. S1) of dissociation transients recorded under 'disperse' ('D', 0.5 μM RAD51) and 'saturated' ('S', 5 μM RAD51) conditions. Areas of symbols are proportional to A_i values (cf. Eq. S1). Results are shown as average values for two datasets.

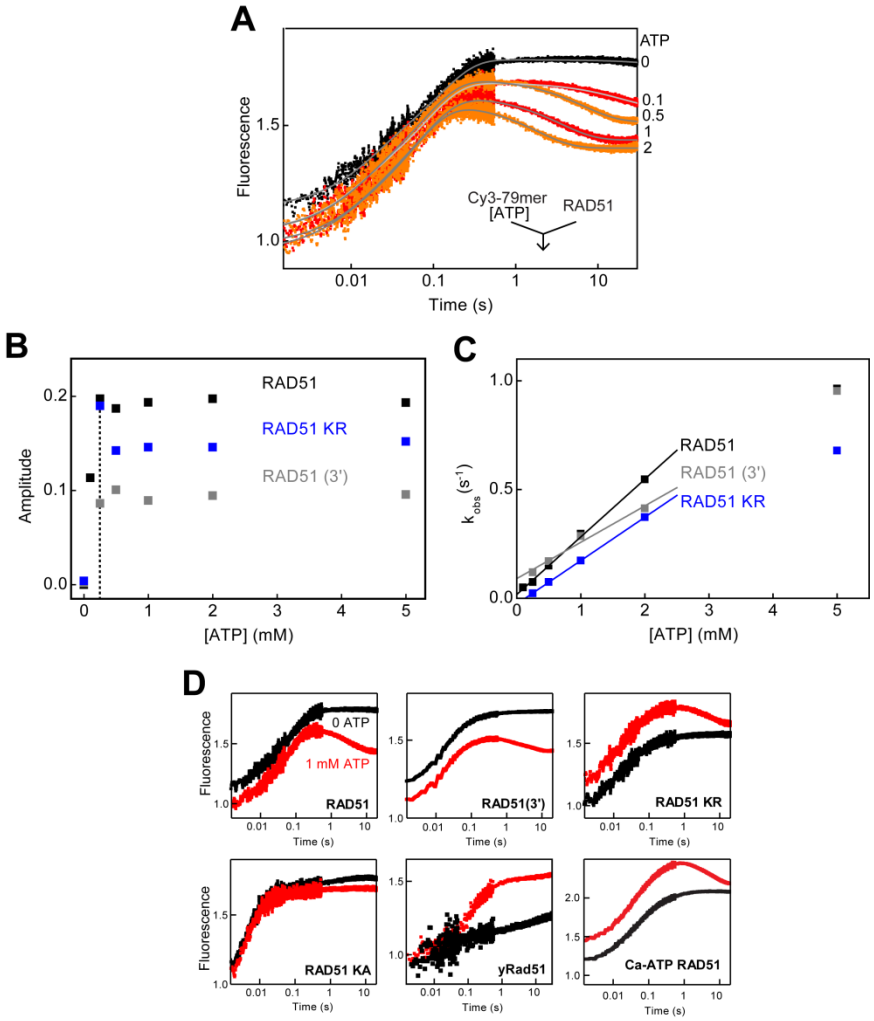

Supplementary Figure S7. The evolutionary differences between yeast and human RAD51**.** (**A**) Stopped-flow Cy3 fluorescence traces recorded upon rapidly mixing 40 nM 5'-Cy3-dT_{79} (3.16 μM nt) with RAD51 WT at increasing concentrations of ATP (top to bottom: 0, 0.1, 0.5, 1, and 2 mM) in the DNA-containing syringe. Tri-exponential best fits (**Eq. S2**) are shown as gray lines. (**B**) ATP concentration dependence of the amplitude of the ATP-mediated fluorescence-decreasing phase shown in panel **A**, expressed relative to the fluorescence level of RAD51-free 5'-Cy3-dT_{79} (or 3'-Cy3-dT_{79} indicated as 3'). Dashed line denotes concentration of ATP where maximal amplitude was already reached. (**C**) ATP concentration dependence of k_{obs} values of the ATP-mediated fluorescence decrease shown in panel **A**. Linear fits in the 0-2 mM ATP concentration regime (solid lines) were used to determine ATP binding k_{on} (slope) values of 0.25 ± 0.01 $mM^{-1}s^{-1}$ (RAD51 WT), 0.20 ± 0.05 $mM^{-1}s^{-1}$ (RAD51 WT 3'), and 0.23 ± 0.06 $mM^{-1}s^{-1}$ (RAD51 KR) (fitting standard errors listed). Fitted k_{off} (intercept) values were lower than 0.1 s^{-1} in all cases. (**D**) Traces recorded upon rapidly mixing 40 nM 5'-Cy3-dT_{79} or 3'-Cy3-dT_{79} (3.16 μM nt) with RAD51 WT, RAD51 KR, RAD51 KA, and yRad51 (5 μM), in the absence (black) and presence (red) of 1 mM ATP in the DNA-containing syringe, in Ca-ATP magnesium was replaced with 1 mM calcium ions. Fluorescence levels are shown relative to that of RAD51-free 5'-Cy3-dT_{79} (or 3'-Cy3-dT_{79} indicated as 3').